The major subunit of widespread competence (pseudo)pili exhibits a novel and conserved type IV pilin fold

Devon Sheppard[1], Jamie-Lee Berry[1], Rémi Denise[2,3], Eduardo P. C. Rocha[2], Stephen J. Matthews[4] and Vladimir Pelicic[1,*]

[1]MRC Centre for Molecular Bacteriology and Infection, Imperial College London, London SW7 2AZ, United Kingdom

[2]Microbial Evolutionary Genomics, Institut Pasteur, CNRS, UMR3525, Paris 75015, France

[3]Sorbonne Université, Collège doctoral, Paris 75005, France

[4]Centre for Structural Biology, Imperial College London, London SW7 2AZ, United Kingdom

*Correspondence: v.pelicic@imperial.ac.uk

ABSTRACT

Type IV filaments (Tff) - a superfamily of filamentous nanomachines virtually ubiquitous in prokaryotes - are helical assemblies of type IV pilins that mediate a wide variety of functions. The competence (Com) (pseudo)pilus is a widespread Tff mediating DNA uptake in bacteria with one membrane (monoderms), which is the first step in natural transformation, an important mechanism of horizontal gene transfer. Here, we report the genomic, phylogenetic and structural analysis of ComGC, the major pilin subunit of Com (pseudo)pili. By performing a global comparative analysis, we show that Com (pseudo)pili are virtually ubiquitous in Bacilli, a major monoderm class of Firmicutes, and ComGC displays extensive sequence conservation, defining a monophyletic group among type IV pilins. We also report two ComGC solution structures from two naturally competent human pathogens, *Streptococcus sanguinis* ($ComGC_{SS}$) and *Streptococcus pneumoniae* ($ComGC_{SP}$), revealing that this pilin displays extensive structural conservation. Strikingly, $ComGC_{SS}$ and $ComGC_{SP}$ exhibit a novel type IV pilin fold, which is purely helical. Modelling of ComGC packing into Tff confirms that its unusual structure is compatible with helical filament assembly. Owing to the widespread distribution of ComGC, these results have implications for hundreds of monoderm species.

Keywords: natural transformation, type IV pilin, type IV filaments, DNA uptake

INTRODUCTION

Filamentous nanomachines composed of type IV pilins are virtually ubiquitous in Bacteria and Archaea (Berry and Pelicic, 2015), to which they confer a variety of unrelated functions including adhesion, motility, protein secretion, DNA uptake. These type IV filaments (Tff) are assembled by conserved multi-protein machineries, which further underlines their phylogenetic relationship (Denise et al., 2019).

Much of our current understanding of this superfamily of nanomachines comes from the study of type IV pili (Tfp), the best characterised Tff (Berry and Pelicic, 2015). In brief, Tfp are µm-long and thin surface-exposed filaments, which are polymers of usually one major type IV pilin. Type IV pilins (simply named pilins hereafter) are defined by an N-terminal sequence motif known as class III signal peptide (Giltner et al., 2012). This motif - IPR012902 entry in the InterPro database (Jones et al., 2014) - consists of a hydrophilic leader peptide ending with a tiny residue (Gly or Ala), followed by a tract of 21 mostly hydrophobic residues, except for a negatively charged Glu_5. This hydrophobic tract represents the N-terminal portion (α1N) of an extended α-helix of ~50 residues (α1), which is the universally conserved structural feature of type IV pilins (Giltner et al., 2012). Although some small pilins consist solely of this extended α-helix (Reardon and Mueller, 2013), most pilins have a globular head consisting of the C-terminal half of α1 (α1C) packed against a β-sheet composed of several antiparallel β-strands, which gives them their typical "lollipop" 3D architecture (Giltner et al., 2012). Upon translocation of prepilins across the cytoplasmic membrane (CM), where they remain embedded via their protruding hydrophobic α1N, the leader peptide is processed by an integral membrane aspartic acid protease named prepilin peptidase (IPR000045) (LaPointe and Taylor, 2000). Processing primes pilins for polymerisation into filaments. Filament assembly, which remains poorly understood, is mediated by a multi-protein machinery in the CM, centred on an integral membrane platform protein (IPR003004) and a cytoplasmic extension ATPase (IPR007831) (Berry and Pelicic, 2015). As revealed by recent

cryo-EM structures of several Tfp (Kolappan et al., 2016; Wang et al., 2017), filaments are right-handed helical polymers where pilins are held together by extensive interactions between their α1 helices, which are partially melted and run approximately parallel to each other within the filament core.

One of the key functional roles of Tff is their involvement in natural transformation in prokaryotes, the ability of species defined as "competent" to take up exogenous DNA across their membrane(s) and incorporate it stably into their genomes (Dubnau and Blokesch, 2019). This widespread property in bacteria (Johnston et al., 2014) is key for horizontal gene transfer, an important factor in bacterial evolution and the spread of antibiotic resistance. Tff are involved in the very first step of natural transformation, *i.e.* binding of free extracellular DNA and its translocation close to the cytoplasmic membrane (Dubnau and Blokesch, 2019). DNA is subsequently bound by the DNA receptor ComEA and further translocated across the CM through the ComEC channel (Dubnau and Blokesch, 2019). In diderm competent species, the Tff involved in DNA uptake is a sub-type of Tfp, known as Tfpa (Berry et al., 2019), which rapid depolymerisation is powered by the retraction ATPase PilT (IPR006321), generating exceptionally large tensile forces (Merz et al., 2000). In brief, Tfpa bind DNA directly, via one of their major or minor (low abundance) pilin subunits (Cehovin et al., 2013), and then are retracted by PilT, bringing DNA to the ComEA receptor (Ellison et al., 2018). In monoderm competent species, DNA uptake is mediated by a distinct Tff named competence (Com) (pseudo)pilus (Dubnau and Blokesch, 2019), much less well characterised than Tfp. Com (pseudo)pili are composed mainly of the major pilin (ComGC) (Chen et al., 2006; Laurenceau et al., 2013), and are assembled by a simple machinery composed of four minor pilins (ComGD, ComGE, ComGF, ComGG), a prepilin peptidase (ComC), an extension ATPase (ComGA) and a platform protein (ComGB) (Chung and Dubnau, 1995, 1998). Com filaments are elusive Tff, since µm-long filaments have been visualised only in *S. pneumoniae* so far (Laurenceau et al.,

2013; Muschiol et al., 2017), while filaments are thought to be much shorter in the other model competent species *Bacillus subtilis* (Chen et al., 2006). For this reason, until this points is addressed in other competent species, we refer to Com as (pseudo)pili in this study.

How Com (pseudo)pili are assembled, bind DNA and presumably retract in the absence of a PilT retraction motor is not understood. One important limitation is the absence of high-resolution structural information. Therefore, in the present study, we have focused on ComGC, the major subunit of the Com (pseudo)pilus. We report (i) a global comparative and phylogenetic analysis of ComGC, and (ii) 3D structures for two orthologs, $ComGC_{SP}$ from the model competent species *S. pneumoniae* and $ComGC_{SS}$ from *S. sanguinis*, a common cause of infective endocarditis in humans that has recently emerged as a monoderm model for the study of Tff. Finally, we discuss the general implications of these findings.

RESULTS

Com (pseudo)pili are almost ubiquitous in monoderm Bacilli, including the Tff model S. sanguinis

So far, Com (pseudo)pili have been mainly studied in two model competent species: *B. subtilis* and *S. pneumoniae*. *S. sanguinis* is a naturally competent species that has recently emerged as a monoderm Tff model since it expresses retractable Tfpa and Com (pseudo)pili (Pelicic, 2019). Functional analysis of *S. sanguinis* Tfpa showed that they are dispensable for DNA uptake, which is instead mediated by the Com (pseudo)pilus since competence was abolished in a *ΔcomGB* mutant (Gurung et al., 2016). A closer inspection of *S. sanguinis* genome revealed that all the genes encoding the Com (pseudo)pilus are present. These genes are organised in two loci (Fig. 1A), *comC* and the *comGABCDEDFG* operon, showing shared synteny with the corresponding loci in model competent species (Albano et al., 1989; Mohan et al., 1989). Multiple sequence alignments of the corresponding proteins with orthologs in *B. subtilis* and *S. pneumoniae* showed extensive conservation (Table S1). Detailed sequence analysis of the N-termini of the five ComG pilins identified clear class III signal peptides (Fig. 1B), *i.e.* with short (8-15 residues) and hydrophilic leader peptides ending with an Ala, followed by a tract of 21 mostly hydrophobic residues. ComGG is the only pilin that does not have a negatively charged Glu_5 and displays a non-canonical class III signal peptide (Fig. 1B), which is not identified by InterPro or PilFind that is dedicated to the prediction of type IV pilins (Imam et al., 2011). This is a conserved property for ComGG orthologs.

We next determined the global distribution of the Com system in publicly available complete bacterial genomes using MacSyFinder (Abby et al., 2014). Specifically, we used the MacSyFinder model built for the identification of Com systems (Denise et al., 2019), which takes into account the genetic composition and organisation of its components. This showed that the Com system is restricted to

Firmicutes, a phylum comprising a vast majority of monoderms, where it is exceptionally widespread since it was detected in 2,333 genomes (Supplemental Spreadsheet 1). An overwhelming majority of the corresponding species (99.7%) belong to the taxonomic class Bacilli (equally distributed among the Bacillales and Lactobacillales orders). As many as 88.7% of the sequenced Bacilli have a Com system. We also detected Com systems in one Clostridia (out of 336) and six Erysipelotrichia (out of 14). In total, 349 different species have the potential to express a Com (pseudo)pilus (Supplemental Spreadsheet 2).

Taken together, these findings suggest that the Com (pseudo)pilus is almost ubiquitous in Bacilli, and can be advantageously studied in the Tff model monoderm species *S. sanguinis*.

ComGC, the major subunit of Com (pseudo)pili, is highly conserved and defines a monophyletic group among type IV pilins

We next focused specifically on the major subunit of Com (pseudo)pili, the pilin ComGC (Chen et al., 2006; Laurenceau et al., 2013). Compared to major pilins from Tfpa, ComGC is ~40% shorter, with 94 or 93 aa for the processed $ComGC_{SS}$ and $ComGC_{SP}$, respectively (10.18 and 10.42 kDa). Moreover, unlike most other pilins, in which the only detectable sequence homology is usually in the α1N portion of the class III signal peptide (Giltner et al., 2012), ComGC orthologs show extensive sequence identity. For example, processed $ComGC_{SS}$ and $ComGC_{SP}$ display 65.6% overall sequence identity (Fig. 2). Similarly, processed $ComGC_{SS}$ and $ComGC_{BS}$ (from *B. subtilis*) show 33.3% sequence identity overall (Fig. S1). This is consistent with the existence of a ComGC signature in the InterPro database (IPR016940) (Jones et al., 2014), which lists 2,809 ComGC entries. Global multiple alignment of these ComGC proteins shows that most of the sequence is conserved in ~90% of the entries (Fig. 2). In Fig. 2, the consensus sequences have been aligned to $ComGC_{SS}$ and $ComGC_{SP}$. Strikingly, some residues show sequence identity in virtually all the

entries, including residues outside of the α1N portion (such as Ala_{38}, Gln_{46}, Tyr_{50} and Leu_{64} in $ComGC_{SS}$), which is highly unusual in type IV pilins.

The above observations suggest that Com (pseudo)pili form a highly homogeneous Tff sub-family. This was tested by performing a phylogenetic analysis based on the protein sequences of major pilins from different Tff found in a wide variety of bacteria, including Tfpa, Tfpb, Tfpc (also known as Tad pili), mannose-sensitive hemagglutinin pili (MSH), type II secretion systems (T2SS) and Com (pseudo)pili. The phylogeny tree that was generated (Fig. 3), using IQ-TREE (Nguyen et al., 2015), reveals that several Tff are in clear monophyletic groups with good branch support, >96% ultrafast bootstrap (UFBoot) (Hoang et al., 2018). Of particular interest, Com (pseudo)pili define a highly supported clade (99% UFBoot), clearly distinct form all other Tff systems.

Taken together, these findings show that ComGC is a small pilin with a highly conserved sequence, which defines a monophyletic group.

Solution structure of two ComGC orthologs reveal a conserved and new type IV pilin fold

Since high-resolution structural information is needed to improve our understanding of Com (pseudo)pili, we decided to solve the 3D structure of $ComGC_{SS}$. To facilitate protein purification, we used a synthetic *comGC*$_{SS}$ gene codon-optimised for expression in *Escherichia coli*, and fused the 72 aa-long soluble portion of $ComGC_{SS}$ to a non-cleavable N-terminal hexahistidine tag (6His). This truncation, which removes the first 22 residues that invariably form a protruding hydrophobic α-helix (α-1N), is known not to affect the structural fold of the rest of the protein (Giltner et al., 2012). The resulting 8.79 kDa 6His-$ComGC_{SS}$ protein could be purified using a combination of affinity and gel-filtration chromatography, as a well-behaved and soluble protein. After purification of isotopically labelled protein with ^{13}C and ^{15}N for backbone and side-chain NMR resonance assignments, we could assign 99.5% of

the backbone and 92% of assignable protons overall. Structural ensembles were determined with 962 NOE based restraints, 50 hydrogen bonds, 110 dihedral angles restraints and 39 residual dipolar couplings (RDC) (Table 1). As can be seen in Fig. 4, ComGC$_{SS}$ 3D structure is unlike that of any type IV pilin present in PDB, as it is purely helical, with three distinct helices connected by loops. The helices present are consistent with JPred secondary structure prediction (Fig. 2) (Drozdetskiy et al., 2015). The N-terminal α1-helix, which involves residues 37-53 of the processed protein, corresponds to α1C since the hydrophobic α1N has been truncated in 6His-ComGC$_{SS}$. Tightly packed against this α1-helix, in a parallel plane, are α2-helix (residues 61-67) and α3-helix (residues 72-85), which stack against each other in antiparallel fashion (Fig. 4A) and orthogonally to α1. Except for the N-terminal unstructured residues, the ComGC$_{SS}$ structures within the NMR ensemble superpose well onto each other (Fig. 4B), with a root mean square deviation (RMSD) of 1.22 Å for Cα atoms, which suggests that there is no significant flexibility in this region of the structure (Krissinel and Henrick, 2004). The unstructured N-terminus, which lacks long and medium NOEs present in the ordered regions of the proteins, was predicted to be highly dynamic based on TALOS+ (Shen et al., 2009), with an average S^2 order parameter of 0.49 ± 0.10.

Our ComGC$_{SS}$ structure differs markedly from the recently reported solution structure of ComGC$_{SP}$ (PDB 5NCA) (Muschiol et al., 2017), which is surprising considering the high sequence identity between these two proteins (Fig. 2). Therefore, in order to define the structural relationship between ComGC orthologs, we decided to solve the structure of ComGC$_{SP}$. As above, we used a synthetic *comGC$_{SP}$* gene codon-optimised for expression in *E. coli*, we fused the 71 aa-long soluble portion of ComGC$_{SP}$ to a non-cleavable N-terminal 6His tag and purified doubly labelled 6His-ComGC$_{SP}$ (8.99 kDa). Again, assignment was excellent since 98.1% of the backbone and 90% of assignable protons overall could be assigned. Structural ensembles were determined with 880 NOE based restraints, 54 hydrogen

bonds, 102 dihedral angles restraints and 38 RDC (Table 1). As can be seen in Fig. 5, our $ComGC_{SP}$ 3D structure is highly similar to the structure of $ComGC_{SS}$, but very different from the solution structure that was recently determined from a low number of restraints (Fig. S2) (Muschiol et al., 2017). In brief, $ComGC_{SP}$ display three distinct helices, with α2-helix (residues 60-66) and α3-helix (residues 71-82) stacking against each other and packing orthogonal to the N-terminal α1-helix (Fig. 5A). As for $ComGC_{SS}$, except for the unstructured N-terminus, there is no significant flexibility in $ComGC_{SP}$ since the structures within the NMR ensemble superpose well onto each other, with a RMSD of 1.60 Å for Cα atoms (Fig. 5B). Our $ComGC_{SS}$ and $ComGC_{SP}$ averaged structures are highly similar (Fig. 5C), with 1.79 Å RMSD between their ordered regions and 1.54 Å RMSD for the helical regions, which is consistent with the high sequence identity between these two proteins.

As determined by GETAREA (Fraczkiewicz and Braun, 1998) with a probe radius of 1.4 Å, the average ratio of solvent exposure for the ordered portion of $ComGC_{SS}$ is 48.3%, relative to 6.7% for those residues determined to be on the interior. In our $ComGC_{SS}$ structure, conserved residues Val_{43}, Gln_{46}, Tyr_{50}, Leu_{64} and Ile_{70} are deeply buried, with an average of only 6.0% solvent exposure, forming a critical portion of an hydrophobic core contributing to the globular fold of ComGC. (Fig. 6). In contrast, conserved Gly_{68} is solvent exposed, which is important for the formation of the α2-helix-turn-α3-helix motif where a tiny residue at the beginning of the turn is necessary to provide the flexibility and lack of steric restrictions required for turning. These observations also apply to our $ComGC_{SP}$ structure, and are surprisingly reflected in the conservation of multiple chemical shifts between the conserved residues in our two structures (Fig. S3). In addition, modelling of the globular head of $ComGC_{BS}$ (Fig. S4), which predicts a globular fold similar to $ComGC_{SS}$ and $ComGC_{SP}$, shows that Cys_{36} and Cys_{76} are in close enough proximity to form a disulfide bond. Such disulfide bond, which is absent in $ComGC_{SS}$ and $ComGC_{SP}$ that do not have Cys residues, is expected to stabilise the globular fold

and was reported to stabilise ComGC in *B. subtilis* (Chen et al., 2006; Meima et al., 2002).

Since the hydrophobic α1N that has been truncated in 6His-ComGC$_{SS}$ is highly similar to the corresponding portion of the PilE major pilin from *Neisseria gonorrhoeae* (Fig. S5), we could model the structure of the portion of α1 truncated in our construct, which produced a reliable model of full-length ComGC$_{SS}$ (Fig. 7). Comparison with the two different pilin folds identified so far - pilins from *N. gonorrhoeae* and *Geobacter sulfurreducens* have been chosen as representative models - clearly shows that ComGC adopts a radically different type IV pilin fold (Fig. 7). All three pilins have in common an extended N-terminal α1-helix, the universal defining structural feature of type IV pilins (Giltner et al., 2012). In addition, while the very short *G. sulfurreducens* pilin almost exclusively consists of α1, both ComGC and PilE display a typical lollipop shape with a globular head mounted onto a "stick" (the α1-helix). However, unlike in canonical pilins where the globular head consists of a 4- to 7-stranded antiparallel β-sheet in a parallel plane to α1, oriented 45° or more relative to the long axis of α1 (Giltner et al., 2012), in ComGC the structural backbone of the globular head is an helix-turn-helix roughly orthogonal to α1 (Fig. 7). While this fold falls within the class of mainly α and the architecture of orthogonal bundles, it represents a novel fold.

Taken together, these structural findings show that ComGC orthologs display conserved 3D structures, with a previously unreported type IV pilin fold.

ComGC novel pilin fold is compatible with helical Tff assembly

Since ComGC represents a novel type IV pilin structural fold, it was important to determine whether it could be modelled into recent cryo-EM structures obtained for a variety of bacterial Tff (Kolappan et al., 2016; Lopez-Castilla et al., 2017; Wang et al., 2017). These structures have revealed that a segment of α1 is melted during filament

assembly, centred on helix-breaking residues Pro_{22} and confirmed that the N-terminal Phe_1 is methylated. Since that portion α1 is highly conserved in ComGC, including the helix-breaking Pro_{22} (Fig. S5), and ComGC has been shown to be N-terminally methylated in *S. pneumoniae* (Laurenceau et al., 2013), we used the PulG pilin from the cryo-EM structure of *Klebsiella oxytoca* T2SS pseudopili (Lopez-Castilla et al., 2017) to produce a reliable full-length 3D structural model of $ComGC_{SS}$ with a melted segment and an N-terminal methyl-Phe_1 (Fig. 8), using SWISS-MODEL (Waterhouse et al., 2018). Apart from these two modifications, this full-length $ComGC_{SS}$ model is very similar to the one in Fig. 7 for which a different template has been used. Considering that ComGC defines a monophyletic group and is highly conserved, it is very likely that all ComGC orthologs will display a similar 3D structure. This was strengthened by producing structural models for a range of different species expressing more or less distant ComGC (21.3-65.6% sequence identity), which were used to generate the phylogeny tree in Fig. 3. As seen in Fig. S6, all the models display the same lollipop shape with a globular head mounted onto a α1 stick. As for $ComGC_{SS}$ and $ComGC_{SP}$, the structural backbone of the globular head is always a helix-turn-helix roughly orthogonal to α1.

We next assessed whether full-length ComGC would be compatible with helical Tff assembly, and found that to be the case. Despite its novel pilin fold, we were able to model packing of ComGC within the cryo-EM structure of *K. oxytoca* T2SS pseudopili, which have a morphology similar to Com (pseudo)pili observed in *S. pneumoniae* (Laurenceau et al., 2013; Muschiol et al., 2017). This produced a homology model with good Ramachandran plot statistics, i.e. allowed (95.3%), generously allowed (3.5%) and disallowed (1.1%) based on PROCHECK (Laskowski et al., 1993). As can be seen in Fig. 8, the model revealed a right-handed helical packing of the conserved N-terminal α1-helices of $ComGC_{SS}$ in the filament core, which run approximately parallel to each other and establish extensive hydrophobic interactions. In addition, the Glu_5 side chain of subunit S establishes a salt bridge and

303 a hydrogen bond with Phe_1 and Thr_2, respectively, of S+1. Importantly, the globular
304 heads are stacked on top of each other along the long axis of the filaments and their
305 helix-turn-helix structural backbone forms the outer surface of the filaments (Fig. 8).

DISCUSSION

Their virtual ubiquity in prokaryotes and role in a variety of key biological processes make Tff an important research topic (Berry and Pelicic, 2015; Denise et al., 2019). Com (pseudo)pili are involved in DNA uptake in naturally competent monoderm bacteria (Dubnau and Blokesch, 2019). Imported DNA, which usually leads to genome diversification via transformation, can also be used as a source of food or as a template for repair of damaged genomic DNA (Johnston et al., 2014). Compared to Tff in diderms, most notably Tfp and T2SS that have been extensively studied, Com (pseudo)pili have been understudied, including from a structural point of view. In this report, we focused on the major subunit of Com (pseudo)pili, the ComGC pilin, which we analysed genomically, phylogenetically and structurally. This led to the notable findings discussed below.

Although Com (pseudo)pili have been primarily studied in two model competent species (*B. subtilis* and *S. pneumoniae*), the present study makes it clear that they are widespread since complete sets of Com-encoding genes are readily detected in more than 2,300 genomes corresponding to almost 350 different species. However, unlike promiscuous Tff such as Tfpa and Tfpc that are found in virtually all phyla of Bacteria (Denise et al., 2019), Com (pseudo)pili are restricted to a single phylum (Firmicutes) and almost exclusively to a single underlying class of monoderms (Bacilli), where they are almost ubiquitous. Indeed, an overwhelming majority of Bacilli genomes (88%) have Com-encoding genes. Interestingly, the major subunit of Com (pseudo)pili (ComGC) shows extensive sequence conservation in the corresponding genomes and define a clear monophyletic group within type IV pilins. Taken together, these observations suggest that the Com (pseudo)pilus is a Tff that has emerged only once, very early during the diversification of Firmicutes, where it has remained largely confined ever since. Since the Com-encoding genes have not become pseudogenes, it is likely that most Bacilli have the ability to assemble a Com (pseudo)pilus and take up DNA. However, since only a handful of these species have

been experimentally shown to be competent (Johnston et al., 2014), this implies that either the imported DNA is primarily used as food or for genome repair instead of genome diversification, or that the inducing cues leading to transformation are yet to be established for most species of Firmicutes. Alternatively, Com (pseudo)pili might have evolved in some of these species to take up other macromolecules, which is however at odds with the conservation of the five pilins.

Perhaps the most important finding in this study is that ComGC, the major subunit of the Com (pseudo)pilus, displays an entirely novel major pilin fold where the extended N-terminal α1-helix, the universal defining structural feature of type IV pilins (Giltner et al., 2012), is topped by a purely helical globular head. ComGC thus appears to be a "middle ground" between longer canonical pilins (e.g. *N. gonorrhoeae*), in which the globular head consists of an antiparallel β-sheet, and the very short pilins where a globular head is missing altogether (e.g. *G. sulfurreducens*). These structures point to a hypothetical evolutionary scenario during which truncation of the antiparallel β-sheet in a canonical type IV pilin might have led to a purely helical ComGC proto-structure. Intriguingly, this scenario "works" particularly well with PilE1, the major subunit of *S. sanguinis* Tfp, which has two short α-helices in the loop connecting α1 and the antiparallel β-sheet (Berry et al., 2019). Importantly, this putative "truncation" does not interfere with the ability of ComGC to be assembled into helical filaments, since ComGC could be readily modelled into recent Tff structures (Kolappan et al., 2016; Lopez-Castilla et al., 2017; Wang et al., 2017). Com (pseudo)pili are thus likely to result from the right-handed helical packing of ComGC α1-helices within the filament core, running parallel to each other and establishing extensive hydrophobic interactions, with a melted central portion. Such packing will stack the globular heads on top of each other, forming the surface of the filaments. Extensive sequence conservation, including for residues which make contacts between chains in our (pseudo)pilus model beyond the classically conserved α1N, and the fact that the two structures that we solved are virtually

identical, strongly suggest that these structural features apply to the whole ComGC clade, including species such as *B. subtilis* where extended filaments have not been observed (Chen et al., 2006). It is therefore surprising that a recently published NMR structure of $ComGC_{SP}$ (PDB 5NCA) (Muschiol et al., 2017) differs dramatically from ours. While the previous structure is purely helical as well, the orientation of the α2 and α3 helices is entirely different, resulting in an absence of packing of the conserved hydrophobic core. Therefore, PDB 5NCA which resembles a one-sided "pick-axe" with no globular head cannot be readily modelled into a helical Tff (Fig. S7). Indeed, the pick-axe points towards the filament core, which is sterically disallowed and incompatible with filament assembly. Interestingly, our assignments vary only slightly from those previously produced for PDB 5NCA (Fig. S8). However, while we have managed to successfully assign 90% assignable protons overall, the previous assignment was merely 65% (Muschiol et al., 2017), which probably accounts for the apparently "unfolded" state of PDB 5NCA. Indeed, without a high degree of proton identification, the assignment of NOESY peaks and production of distance restraints fails. Local hydrogen bonds and dihedral restraints often cannot compensate for lack of long-range NOEs within the protein interior or between elements of secondary structure.

Together with these conserved structural features, the conservation *en bloc* of the genes encoding the Com (pseudo)pilus strongly suggests that the molecular mechanisms of filament assembly and DNA uptake are widely conserved in Firmicutes. These mechanisms, which remain poorly understood, can be advantageously studied in *S. sanguinis*, which has recently emerged as a monoderm Tfp model (Pelicic, 2019). Actually, *S. sanguinis* is the only monoderm shown to express two distinct Tff, retractable Tfpa and Com (pseudo)pili, which further cements it as a prime Tff model species. Comparison with other Tff systems shows that the machinery involved in biogenesis of Com (pseudo)pili is one of the simplest, by far. Since ComGD, ComGE, ComGF and ComGG pilins are likely to be minor

(pseudo)pilus components important for filament stability and function (a conserved role for minor pilins in various Tff) (Berry and Pelicic, 2015), and ComC is the prepilin peptidase processing pilins (Chung et al., 1998), it appears that assembly of ComGC into filaments is mediated by two proteins only. Namely, an extension ATPase (ComGA) and a platform protein (ComGB), which together will assemble processed ComGC in a right-handed helical filament. Upon DNA binding, which has been visualised for *S. pneumoniae* Com (pseudo)pili, but the receptor is yet to be identified (Laurenceau et al., 2013), uptake will be initiated by filament retraction (Ellison et al., 2018). Since there is no dedicated retraction ATPase, ComGA might therefore be a bifunctional motor powering both extension and retraction like recently suggested for the Tfpc motor (Ellison et al., 2019). It would be interesting to image Com filaments dynamics and DNA-binding ability in live cells, using a labelling strategy that has recently enabled the visualisation of these steps for Tfpa involved in competence in naturally competent diderm species (Ellison et al., 2018).

In conclusion, by providing high-resolution structural information for the ComGC pilins, this study has shed light on an understudied Tff involved in DNA uptake found in hundreds of monoderm bacterial species and has led to the surprising discovery of a novel type IV pilin fold. This paves the way for further investigations of this minimalist Tff, which are expected to improve our understanding of a fascinating superfamily of filamentous nanomachines ubiquitous in prokaryotes.

EXPERIMENTAL PROCEDURES

Bioinformatic analyses

Protein sequences were routinely analysed using the DNA Strider program. Protein sequence alignments were done using the Clustal Omega server at EMBL-EBI. Pretty-printing of alignment files was done using BoxShade server at ExPASy. Reformatting of large multiple alignment files was done using the MView server at EMBL-EBI. Prediction of functional domains was done using the InterProScan server at EMBL-EBI, which was also used to download all the ComGC protein entries with an IPR0160940 domain. Protein secondary structure prediction was done using JPred server at University of Dundee. Protein 3D structures were downloaded from the RCSB PDB server. Molecular visualisation of protein 3D structures was done using PyMOL (Schrödinger). The GETAREA server, at UTMB, was used for calculating the solvent accessible surface area of ComGC proteins.

Detection of the Com systems in genomes available in NCBI RefSeq database (last accessed in April 2019, 13,512 genomes of Bacteria and Archaea) was done as described previously (Denise et al., 2019), using MacSyFinder (Abby et al., 2014) and the relevant HMM Com model (Denise et al., 2019). Phylogenetic analysis based on protein sequences of major pilins of different Tff involved an initial alignment of the sequences using MAFFT v7.273 (Katoh and Standley, 2013), specifically the linsi algorithm. Multiple alignments were analysed using Noisy v1.5.12 (Dress et al., 2008) with default parameters, in order to select the informative sites. Next, we inferred maximum likelihood trees from the curated alignments using IQ-TREE v 1.6.7.2 (Nguyen et al., 2015), with option -allnni. We evaluated the node supports using the options -bb 1,000 for ultra-fast bootstraps, and -alrt 1,000 for SH-aLRT (Hoang et al., 2018). The best evolutionary model was selected with ModelFinder (Kalyaanamoorthy et al., 2017), option -MF and BIC criterion. We used the option -wbtl to conserve all optimal trees and their branches length.

438

439 **Protein expression and purification**

440 A synthetic gene, codon-optimised for *E. coli* expression, encoding $ComGC_{SS}$ from *S.*
441 *sanguinisis* 2908 (Gurung et al., 2016) was synthesised and cloned by GeneArt,
442 yielding pMA-T-*comGC*$_{SS}$ (Table S2). The portion of the gene encoding residues 23-
443 94 from the mature protein was PCR-amplified using *comGC*$_{SS}$-F and *comGC*$_{SS}$-R
444 primers (Table S3), cut with NcoI and BamHI and cloned into the pET28b vector
445 (Novagen) cut with the same enzymes. The forward primer was designed to fuse a
446 non-cleavable N-terminal 6His tag to $ComGC_{SS}$. The resulting plasmid was verified
447 by sequencing and transformed into chemically competent *E. coli* BL21(DE3) cells. A
448 single colony was transferred to 10 ml of LB supplemented with 50 $\mu g.ml^{-1}$
449 kanamycin and grown at 37°C overnight (O/N). This pre-culture was back-diluted
450 100-fold into 1 l M9 minimal medium, supplemented with antibiotic, a mixture of
451 vitamins and trace elements, and ^{13}C D-glucose and ^{15}N NH_4Cl for isotopic labelling.
452 Cells were grown in an orbital shaker at 37°C until the OD_{600} reached 0.7, before
453 adding 0.4 mM IPTG (Merck Chemicals) to induce protein expression during 16 h at
454 18°C. Cells were then harvested by centrifugation at 8,000 *g* for 20 min and
455 subjected to one freeze/thaw cycle in lysis buffer (PBS pH 7.4, with EDTA-free
456 protease inhibitors). This lysate was further disrupted by repeated cycles of
457 sonication, pulses of 5 sec on and 5 sec off during 5 min, until the cell suspension
458 was visibly less viscous. The cell lysate was then centrifuged for 20 min at 18,000 *g*
459 to remove cell debris. The clarified lysate was then passed using an ÄKTA Purifier
460 FPLC through a 1 ml HisTrap HP column (GE Healthcare), pre-equilibrated in lysis
461 buffer. The column was then washed extensively with lysis buffer to remove unbound
462 material before 6His-$ComGC_{SS}$ was eluted using elution buffer (PBS pH 7.4, 200 mM
463 NaCl, 300 mM imidazole). Affinity-purified $ComGC_{SS}$ was further purified by gel-
464 filtration chromatography on an HiLoad 16/600 Superdex 75 column (GE

Healthcare), using (25 mM Na_2HPO_4/NaH_2PO_4 pH 6, 200 mM NaCl) buffer for elution. For RDC measurements we produced ^{15}N labelled protein as follows. Bacteria grown O/N in 5 ml LB with antibiotic were sub-cultured at 37ºC in 0.8 l LB to 0.6 OD_{600}, and then transferred to 0.4 l M9 with ^{15}N NH_4Cl, unlabelled D-glucose, and 10 $\mu g.l^{-1}$ thiamine. Cultures were induced with 0.3 mM IPTG at 16ºC for 18 h. After the production of a clarified lysate, protein was purified as above, except for the use of hand-made Ni-NTA agarose (Qiagen) in (50 mM Tris pH 8, 300 mM NaCl) and eluted using (50 mM Tris pH 8, 200 mM NaCl, 300 mM imidazole), and Superdex 75 10/300 GL (GE Healthcare) columns in (25 mM Tris pH 8, 200 mM NaCl) and dialysed into (25 mM Na_2HPO_4/NaH_2PO_4 pH 6, 50 mM NaCl).

For $ComGC_{SP}$, a codon-optimised synthetic gene based on the gene from *S. pneumoniae* R6 was synthesised and cloned by GeneArt, yielding pMA-T-*comGC*$_{SP}$ (Table S2). The portion of the gene encoding residues 23-93 from the mature protein was PCR-amplified using *comGC*$_{SP}$-F and *comGC*$_{SP}$-R primers (Table S3), cut with NcoI and BamHI and cloned into the pET28b vector (Novagen) cut with the same enzymes. The forward primer was designed to fuse a non-cleavable N-terminal 6His tag to $ComGC_{SS}$. The resulting plasmid was verified by sequencing and transformed into chemically competent *E. coli* BL21(DE3) cells. A single colony was transferred to 5 ml of LB supplemented with 50 $\mu g.ml^{-1}$ kanamycin and grown O/N at 37°C. Bacteria were sub-cultured at 37ºC in 0.8 l LB with antibiotic to OD_{600} 0.7, and then transferred into 0.4 l M9 with10 $\mu g.l^{-1}$ thiamine, and either ^{15}N NH_4Cl and unlabelled D-glucose, or ^{15}N NH_4Cl and ^{13}C D-glucose. Cultures were induced with 0.3 mM IPTG at 16ºC for 18 h. After the production of a clarified lysate, $ComGC_{SS}$ was purified as above using hand-made Ni-NTA agarose (Qiagen) and Superdex 75 10/300 GL (GE Healthcare) columns.

NMR spectroscopy and structure determination

All data was collected on Bruker Avance III HD 800 MHz and 600 MHz triple resonance spectrometers with cryoprobes operated at 25ºC. For $ComGC_{SS}$, a sample containing ^{13}C, ^{15}N labelled protein at 1 mM in NMR buffer (25 mM Na_2HPO_4/NaH_2PO_4 pH 6, 50 mM NaCl, 5% D_2O) was used for assignment experiments and structure determination. For $ComGC_{SP}$, a sample containing ^{13}C, ^{15}N labelled protein at 1.8 mM in NMR buffer was used for assignment experiments and structure determination. Resonance assignments for $ComGC_{SS}$ were performed using ^{15}N HSQC, ^{13}C aliphatic HSQC, HNCACB, CBCACONH, HBHA, HNCO, HNCACO, HCCCONH, CCCONH and CCH. For $ComGC_{SP}$, assignments were performed using ^{15}N HSQC, ^{13}C aliphatic HSQC, HNCA, CBCANH, CBCACONH, HBHA, HNCO, HNCACO, HCCCONH, CCCONH and CCH. All data was processed using MddNMR (Orekhov and Jaravine, 2011) for reconstruction after Non-Uniform Sampling and NMRPipe (Delaglio et al., 1995). Peak picking and assignments were performed in SPARKY (Lee et al., 2015).

NOE peak lists were used, with mixing time of 140 msec, from 3D ^{13}C HSQC-NOESY, 3D ^{15}N HSQC-NOESY for $ComGC_{SP}$, and simultaneous $^{13}C/^{15}N$ chemical shift evolution NOESY for $ComGC_{SS}$. For both proteins, RDC lists were derived from ^{15}N HSQC-IPAP experiments on ^{15}N labelled isotropic and aligned sample in 3% PEG/hexanol liquid crystal, with D_2O splitting of ~7 Hz. RDCs were included in the structure calculations if there was baseline resolution and for residues where TALOS+ predicted order parameter of >0.8. Angular constraints from TALOS+ were used in the structure calculations. Both $ComGC_{SS}$ and $ComGC_{SP}$ structures were determined using Ponderosa-C/S (Lee et al., 2015), refined using Xplor-NIH 2.52 (Schwieters et al., 2006), aligned using Theseus (Theobald and Wuttke, 2008), and secondary structure checked using Stride (Frishman and Argos, 1995). Structure validation was performed using PSVS (Bhattacharya et al., 2007), PROCHECK (Laskowski et al., 1993) and in-house scripts.

Modelling

SWISS-MODEL server at ExPASy was used for modelling protein 3D structures. In brief, the full-length ComGC$_{SS}$ was modelled with using *N. gonorrhoeae* major pilin (PDB 2PIL) as a template (Forest et al., 1999). We first modelled the missing α1 residues in our structure, which was aligned to our Xplor-NIH-produced average NMR structure (without the first unstructured α1 residues) using PyMol and finally merged using Coot (Emsley et al., 2010).

Similarly, the full-length ComGC$_{SS}$ structure within filaments was modelled by using one *K. oxytoca* PulG subunit from the T2SS pseudopilus (PDB 5WDA) as a template for the missing α1 residues in our structure (Lopez-Castilla et al., 2017). This full-length ComGC$_{SS}$ was then used to produce models of a variety of more or less distant ComGC orthologs. The Com (pseudo)pilus model was produced after alignment of the averaged NMR structure ComGC α1-helices to the α1-helices of SWISS-MODEL PulG-based homology model subunits in the T2SS pseudopilus. This was also done for the recently published ComGC$_{SP}$ structure (PDB 5NCA). The structures were fused and we added the N-terminal methyl-Phe$_1$ using Coot (Emsley et al., 2010). In addition, we modelled packing of full-length ComGC$_{SS}$ in the PAK pilus from *P. aeruginosa* (PDB 5VXY) (Wang et al., 2017).

ACCESSION NUMBERS

The NMR solution structures of $ComGC_{SS}$ and $ComGC_{SP}$ have been deposited in the Protein Data Bank under entries 6TXT and 6Y1H, respectively. Chemical shift assignments and NOE-based restraints used in structure calculations are available from the BMRB under accession numbers 50194 and 7441, respectively.

AUTHOR CONTRIBUTIONS

V.P. designed the research. E.P.C.R., S.J.M. and V.P. directed the research. Experiments were done by D.S., J.L.B and R.D. All authors contributed to writing the manuscript.

ACKNOWLEDGMENTS

This work was funded by a Medical Research Council grant (MR/P022197/1) to V.P. R.D. was funded by the doctoral school Complexité du vivant-ED515 (contract number 2449/2016). E.P.C.R. was funded by the INCEPTION project (PIA/ANR-16-CONV-0005). This work relied heavily on the use of the Cross-Faculty NMR Centre at Imperial College London. We are grateful to Nicolas Biais (City University of New York) and Romé Voulhoux (CNRS Marseille) for critical reading of the manuscript.

REFERENCES

Abby, S.S., Neron, B., Menager, H., Touchon, M., and Rocha, E.P. (2014). MacSyFinder: a program to mine genomes for molecular systems with an application to CRISPR-Cas systems. PLoS One *9*, e110726.

Albano, M., Breitling, R., and Dubnau, D.A. (1989). Nucleotide sequence and genetic organization of the *Bacillus subtilis comG* operon. J Bacteriol *171*, 5386-5404.

Berry, J.L., Gurung, I., Anonsen, J.H., Spielman, I., Harper, E., Hall, A.M.J., Goosens, V.J., Raynaud, C., Koomey, M., Biais, N.*, et al.* (2019). Global biochemical and structural analysis of the type IV pilus from the Gram-positive bacterium *Streptococcus sanguinis*. J Biol Chem *294*, 6796-6808.

Berry, J.L., and Pelicic, V. (2015). Exceptionally widespread nano-machines composed of type IV pilins: the prokaryotic Swiss Army knives. FEMS Microbiol Rev *39*, 134-154.

Bhattacharya, A., Tejero, R., and Montelione, G.T. (2007). Evaluating protein structures determined by structural genomics consortia. Proteins *66*, 778-795.

Cehovin, A., Simpson, P.J., McDowell, M.A., Brown, D.R., Noschese, R., Pallett, M., Brady, J., Baldwin, G.S., Lea, S.M., Matthews, S.J.*, et al.* (2013). Specific DNA recognition mediated by a type IV pilin. Proc Natl Acad Sci USA *110*, 3065-3070.

Chen, I., Provvedi, R., and Dubnau, D. (2006). A macromolecular complex formed by a pilin-like protein in competent *Bacillus subtilis*. J Biol Chem *281*, 21720-21727.

Chung, Y.S., Breidt, F., and Dubnau, D. (1998). Cell surface localization and processing of the ComG proteins, required for DNA binding during transformation of *Bacillus subtilis*. Mol Microbiol *29*, 905-913.

Chung, Y.S., and Dubnau, D. (1995). ComC is required for the processing and translocation of ComGC, a pilin-like competence protein of *Bacillus subtilis*. Mol Microbiol *15*, 543-551.

580 Chung, Y.S., and Dubnau, D. (1998). All seven *comG* open reading frames are
581 required for DNA binding during transformation of competent *Bacillus subtilis*. J
582 Bacteriol *180*, 41-45.
583 Delaglio, F., Grzesiek, S., Vuister, G.W., Zhu, G., Pfeifer, J., and Bax, A. (1995).
584 NMRPipe: a multidimensional spectral processing system based on UNIX pipes. J
585 Biomol NMR *6*, 277-293.
586 Denise, R., Abby, S.S., and Rocha, E.P.C. (2019). Diversification of the type IV
587 filament superfamily into machines for adhesion, protein secretion, DNA uptake, and
588 motility. PLoS Biol *17*, e3000390.
589 Dress, A.W., Flamm, C., Fritzsch, G., Grunewald, S., Kruspe, M., Prohaska, S.J., and
590 Stadler, P.F. (2008). Noisy: identification of problematic columns in multiple
591 sequence alignments. Algorithm Mol Biol *3*, 7.
592 Drozdetskiy, A., Cole, C., Procter, J., and Barton, G.J. (2015). JPred4: a protein
593 secondary structure prediction server. Nucleic Acids Res *43*, W389-W394.
594 Dubnau, D., and Blokesch, M. (2019). Mechanisms of DNA uptake by naturally
595 competent bacteria. Annu Rev Genet *53*, 217-237.
596 Ellison, C.K., Dalia, T.N., Vidal Ceballos, A., Wang, J.C., Biais, N., Brun, Y.V., and
597 Dalia, A.B. (2018). Retraction of DNA-bound type IV competence pili initiates DNA
598 uptake during natural transformation in *Vibrio cholerae*. Nat Microbiol *3*, 773-780.
599 Ellison, C.K., Kan, J., Chlebek, J.L., Hummels, K.R., Panis, G., Viollier, P.H., Biais,
600 N., Dalia, A.B., and Brun, Y.V. (2019). A bifunctional ATPase drives tad pilus
601 extension and retraction. Sci Adv *5*, eaay2591.
602 Emsley, P., Lohkamp, B., Scott, W.G., and Cowtan, K. (2010). Features and
603 development of Coot. Acta Crystallogr Sect D: Biol Crystallogr *66*, 486-501.
604 Forest, K.T., Dunham, S.A., Koomey, M., and Tainer, J.A. (1999). Crystallographic
605 structure reveals phosphorylated pilin from *Neisseria*: phosphoserine sites modify
606 type IV pilus surface chemistry and fibre morphology. Mol Microbiol *31*, 743-752.

607 Fraczkiewicz, R., and Braun, W. (1998). Exact and efficient analytical calculation of
608 the accessible surface areas and their gradients for macromolecules. J Comput
609 Chem *19*, 319-333.
610 Frishman, D., and Argos, P. (1995). Knowledge-based protein secondary structure
611 assignment. Proteins *23*, 566-579.
612 Giltner, C.L., Nguyen, Y., and Burrows, L.L. (2012). Type IV pilin proteins: versatile
613 molecular modules. Microbiol Mol Biol Rev *76*, 740-772.
614 Gurung, I., Spielman, I., Davies, M.R., Lala, R., Gaustad, P., Biais, N., and Pelicic, V.
615 (2016). Functional analysis of an unusual type IV pilus in the Gram-positive
616 *Streptococcus sanguinis*. Mol Microbiol *99*, 380-392.
617 Hoang, D.T., Chernomor, O., von Haeseler, A., Minh, B.Q., and Vinh, L.S. (2018).
618 UFBoot2: improving the ultrafast bootstrap approximation. Mol Biol Evol *35*, 518-522.
619 Imam, S., Chen, Z., Roos, D.S., and Pohlschröder, M. (2011). Identification of
620 surprisingly diverse type IV pili, across a broad range of Gram-positive bacteria.
621 PLoS One *6*, e28919.
622 Johnston, C., Martin, B., Fichant, G., Polard, P., and Claverys, J.P. (2014). Bacterial
623 transformation: distribution, shared mechanisms and divergent control. Nat Rev
624 Microbiol *12*, 181-196.
625 Jones, P., Binns, D., Chang, H.Y., Fraser, M., Li, W., McAnulla, C., McWilliam, H.,
626 Maslen, J., Mitchell, A., Nuka, G., *et al.* (2014). InterProScan 5: genome-scale
627 protein function classification. Bioinformatics *30*, 1236-1240.
628 Kalyaanamoorthy, S., Minh, B.Q., Wong, T.K.F., von Haeseler, A., and Jermiin, L.S.
629 (2017). ModelFinder: fast model selection for accurate phylogenetic estimates. Nat
630 Methods *14*, 587-589.
631 Katoh, K., and Standley, D.M. (2013). MAFFT multiple sequence alignment software
632 version 7: improvements in performance and usability. Mol Biol Evol *30*, 772-780.
633 Kolappan, S., Coureuil, M., Yu, X., Nassif, X., Egelman, E.H., and Craig, L. (2016).
634 Structure of the *Neisseria meningitidis* type IV pilus. Nat Commun *7*, 13015.

635 Krissinel, E., and Henrick, K. (2004). Secondary-structure matching (SSM), a new
636 tool for fast protein structure alignment in three dimensions. Acta Crystallogr Sect D:
637 Biol Crystallogr *60*, 2256-2268.
638 LaPointe, C.F., and Taylor, R.K. (2000). The type 4 prepilin peptidases comprise a
639 novel family of aspartic acid proteases. J Biol Chem *275*, 1502-1510.
640 Laskowski, R.A., W., M.M., Moss, D.S., and Thornton, J.M. (1993). PROCHECK - a
641 program to check the stereochemical quality of protein structures. J Appl Crystallogr
642 *26*, 283-291.
643 Laurenceau, R., Pehau-Arnaudet, G., Baconnais, S., Gault, J., Malosse, C.,
644 Dujeancourt, A., Campo, N., Chamot-Rooke, J., Le Cam, E., Claverys, J.P.*, et al.*
645 (2013). A type IV pilus mediates DNA binding during natural transformation in
646 *Streptococcus pneumoniae*. PLoS Pathog *9*, e1003473.
647 Lee, W., Tonelli, M., and Markley, J.L. (2015). NMRFAM-SPARKY: enhanced
648 software for biomolecular NMR spectroscopy. Bioinformatics *31*, 1325-1327.
649 Lopez-Castilla, A., Thomassin, J.L., Bardiaux, B., Zheng, W., Nivaskumar, M., Yu, X.,
650 Nilges, M., Egelman, E.H., Izadi-Pruneyre, N., and Francetic, O. (2017). Structure of
651 the calcium-dependent type 2 secretion pseudopilus. Nat Microbiol *2*, 1686-1695.
652 Meima, R., Eschevins, C., Fillinger, S., Bolhuis, A., Hamoen, L.W., Dorenbos, R.,
653 Quax, W.J., van Dijl, J.M., Provvedi, R., Chen, I.*, et al.* (2002). The *bdbDC* operon of
654 *Bacillus subtilis* encodes thiol-disulfide oxidoreductases required for competence
655 development. J Biol Chem *277*, 6994-7001.
656 Merz, A.J., So, M., and Sheetz, M.P. (2000). Pilus retraction powers bacterial
657 twitching motility. Nature *407*, 98-102.
658 Mohan, S., Aghion, J., Guillen, N., and Dubnau, D. (1989). Molecular cloning and
659 characterization of *comC*, a late competence gene of *Bacillus subtilis*. J Bacteriol
660 *171*, 6043-6051.
661 Muschiol, S., Erlendsson, S., Aschtgen, M.S., Oliveira, V., Schmieder, P., de
662 Lichtenberg, C., Teilum, K., Boesen, T., Akbey, U., and Henriques-Normark, B.

(2017). Structure of the competence pilus major pilin ComGC in *Streptococcus pneumoniae*. J Biol Chem *292*, 14134-14146.

Nguyen, L.T., Schmidt, H.A., von Haeseler, A., and Minh, B.Q. (2015). IQ-TREE: a fast and effective stochastic algorithm for estimating maximum-likelihood phylogenies. Mol Biol Evol *32*, 268-274.

Orekhov, V.Y., and Jaravine, V.A. (2011). Analysis of non-uniformly sampled spectra with multi-dimensional decomposition. Prog Nucl Mag Res Spect *59*, 271-292.

Pelicic, V. (2019). Monoderm bacteria: the new frontier for type IV pilus biology. Mol Microbiol *112*, 1674-1683.

Reardon, P.N., and Mueller, K.T. (2013). Structure of the type IVa major pilin from the electrically conductive bacterial nanowires of *Geobacter sulfurreducens*. J Biol Chem *288*, 29260-29266.

Schwieters, C.D., Kuszewski, J.J., and Clore, G.M. (2006). Using Xplor-NIH for NMR molecular structure determination. Prog Nucl Mag Res Spect *48*, 47-62.

Shen, Y., Delaglio, F., Cornilescu, G., and Bax, A. (2009). TALOS+: a hybrid method for predicting protein backbone torsion angles from NMR chemical shifts. J Biomol NMR *44*, 213-223.

Theobald, D.L., and Wuttke, D.S. (2008). Accurate structural correlations from maximum likelihood superpositions. PLoS Comput Biol *4*, e43.

Wang, F., Coureuil, M., Osinski, T., Orlova, A., Altindal, T., Gesbert, G., Nassif, X., Egelman, E.H., and Craig, L. (2017). Cryoelectron microscopy reconstructions of the *Pseudomonas aeruginosa* and *Neisseria gonorrhoeae* type IV pili at sub-nanometer resolution. Structure *25*, 1423-1435.

Waterhouse, A., Bertoni, M., Bienert, S., Studer, G., Tauriello, G., Gumienny, R., Heer, F.T., de Beer, T.A.P., Rempfer, C., Bordoli, L.*, et al.* (2018). SWISS-MODEL: homology modelling of protein structures and complexes. Nucleic Acids Res *46*, W296-W303.

690 **LEGENDS TO FIGURES**

691

692 **Fig. 1. Com (pseudo)pilus machinery in *S. sanguinis*.** (**A**) Genomic organisation
693 of the genes involved in the biogenesis of the Com (pseudo)pilus in *S. sanguinis*
694 2908. All the genes are drawn to scale, with the scale bar representing 500 bp. The
695 names of the corresponding proteins are listed at the bottom. (**B**) Sequence
696 alignment of the putative N-terminal class III signal peptides of the five ComG pilins
697 in *S. sanguinis* 2908. The 8-15 aa-long leader peptides, which contain a majority of
698 hydrophilic (shaded in grey) or neutral (no shading) residues, end with a conserved
699 Ala_{-1}. Leader peptides are processed (indicated by the vertical arrow) by the prepilin
700 peptidase ComC. The mature proteins start with a tract of 21 predominantly
701 hydrophobic residues (shaded in black), which invariably form the protruding N-
702 terminal portion of an extended α-helix that is the main assembly interface within
703 filaments.

704

705 **Fig. 2. Global sequence analysis of ComGC pilins.** Sequence alignments of
706 ComGC in *S. sanguinis* and *S. pneumoniae* is represented in the top two rows.
707 Residues were shaded in black (identical), grey (conserved) or unshaded (different).
708 The leader peptide is highlighted. In the recombinant proteins that were produced for
709 structure determination, the N-terminal 22 residues invariably forming a protruding
710 hydrophobic α-helix were truncated (depicted by an arrow) to promote solubility. The
711 2D structural motifs predicted using JPred are depicted in the third row. Fourth and
712 fifth rows represent the 80 and 90% ComGC consensus sequences, computed from
713 2,809 ComGC entries in InterPro, and aligned to $ComGC_{SS}$ and $ComGC_{SP}$. Multiple
714 alignments were generated using Clustal Omega and formatted with MView. Polar:
715 C, D, E, H, K, N, Q, R, S or T. Tiny: A or G. Hydrophobic: A, C, F, G, H, I, K, L, M, R,
716 T, V, W or Y. Aliphatic: I, L or V. Turn-like: A, C, D, E, G, H, K, N, Q, R, S or T. Small:
717 A, C, D, G, N, P, S, T or V.

718

719 **Fig. 3. Rooted phylogeny of the major pilins from various bacterial Tff.** The tree
720 was build using IQ-Tree, with 1,000 replicates of UFBoot and LG+F+R4 model.
721 Numeric values (in %) indicate UFBoot of the corresponding branches. The colour of
722 the bullet points indicates the taxonomic group of the corresponding species. The
723 colour of the strips and highlights indicate the classification of the different Tff
724 systems. Tfpa: type IVa pilus. Tfpb: type IVb pilus. Tfpc: type IVc pilus (also known
725 as Tad). MSH: mannose-sensitive hemagglutinin pilus. Com: competence
726 (pseudo)pilus. T2SS: type II secretion system pseudopilus.

727

728 **Fig. 4. 3D solution structure of ComGC$_{SS}$.** (**A**) Cartoon representation of the
729 ComGC$_{SS}$ structure: face and side views are shown. A dimmed surface
730 representation of the protein is superimposed. The three consecutive α-helices have
731 been named α1, α2 and α3, and highlighted in blue (α1) or cyan (α2 and α3). (**B**)
732 Cartoon representation of the superposition of the ensemble of 10 ComGC$_{SS}$
733 structures determined by NMR, which highlights that there is no significant flexibility
734 in the structure except for the unstructured N-terminus.

735

736 **Fig. 5. 3D solution structure of ComGC$_{SP}$.** (**A**) Cartoon representation of the
737 ComGC$_{SP}$ structure: face and side views are shown. A dimmed surface
738 representation of the protein is superimposed. Nomenclature and colour scheme are
739 the same than in Fig. 4. (**B**) Cartoon representation of the superposition of the
740 ensemble of 10 ComGC$_{SP}$ structures determined by NMR, (**C**) Cartoon
741 representation of the overlay of ComGC$_{SP}$ and ComGC$_{SS}$ representative structures.
742 This highlights the high structural similarity between the two proteins, with 1.54 Å
743 RMSD for the helical regions.

744

Fig. 6. Conserved residues contributing to the globular fold of ComGC. Cartoon representation of the ordered portion of $ComGC_{SS}$, where residues determined to be on the interior using GETAREA - with accessible surface accessibility ratios of less than 20% - are highlighted in orange. The consensus residues Val_{43}, Gln_{46}, Tyr_{50}, Leu_{64} and Ile_{70} are shown with space filling representation.

Fig. 7. ComGC display a novel type IV pilin fold. 3D structure of the three different structural types of type IV pilins identified so far. The canonical type IV pilin fold is represented by the major pilin of Tfpa in *N. gonorrhoeae* (PDB 2PIL). *G. sulfurreducens* Tfpa pilin (PDB 2M7G) is the representative member of the very short pilins almost exclusively consisting of α1. The full-length 3D structure of $ComG_{SS}$ has been modelled. The conserved α1 in all three sub-types is highlighted in blue. Distinctive structural features in the globular heads of PilE (antiparallel β-sheet) and ComGC (antiparallel α2-α3 orthogonal to α1) have been highlighted in cyan.

Fig. 8 3D model of ComGC filaments. The cryo-EM structure of the *K. oxytoca* PulG T2SS pseudopilus (PDB 5WDA) has been used as a template to generate models of $ComGC_{SS}$ (pseudo)pili. (**A**) Full-length $ComGC_{SS}$ in filaments with a melted segment in α1N and an N-terminal methyl-Phe_1. (**B**) $ComGC_{SS}$ (pseudo)pili with a right-handed helical packing of the conserved α1-helices which run approximately parallel to each other in the filament core. (**C**) Top and bottom views of $ComGC_{SS}$ (pseudo)pili highlighting the extensive interactions between α1-helices and the globular heads forming the outer surface of the filaments.

768 **Table 1. NMR structural statistics.**

	$ComGC_{SS}$	$ComGC_{SP}$
NOE-derived distance constraints		
long [(i-j) > 5]	128	95
medium [5 ≥ (i-j) > 1]	414	404
intraresidue (i=j)	420	381
total	962	880
hydrogen bonds	50	54
dihedral constraints (Φ and Ψ)	110	102
residual dipolar couplings (RDC)	39	38
Ramachandran statistics (from PROCHECK)		
most favoured (%)	93.4	83.0
additionally allowed (%)	6.4	15.9
generously allowed (%)	0.2	1.1
disallowed (%)	0.0	0.0
Structure statistics		
RMSD backbone (all residues)	3.3	4.0
RMSD backbone (ordered residues*)	0.6	0.8
RMS bond angles (°)	1.8	1.9
RMS bond lengths (Å)	0.012	0.017
Restraint statistics (RMSD of violations)		
NOE restraints	0.060 ± 0.003	0.179 ± 0.008
hydrogen bonds	0.075 ± 0.015	0.100 ± 0.017
dihedral restraints	1.805 ± 0.075	1.827 ± 0.318
RDC	0.748 ± 0.138	0.716 ± 0.256
Q value	0.146 ± 0.028	0.150 ± 0.054

769 *PROCHECK ordered residues are 37-53, 61-66 and 72-85 for $ComGC_{SS}$, and 36-

770 54, 60-65 and 71-82 for $ComGC_{SP}$.

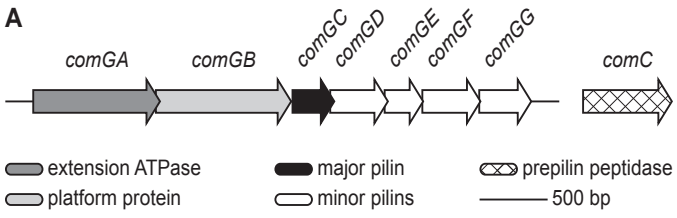

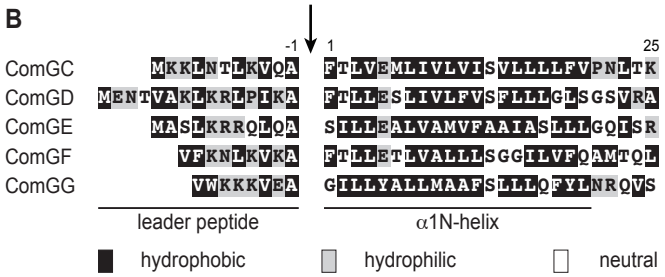

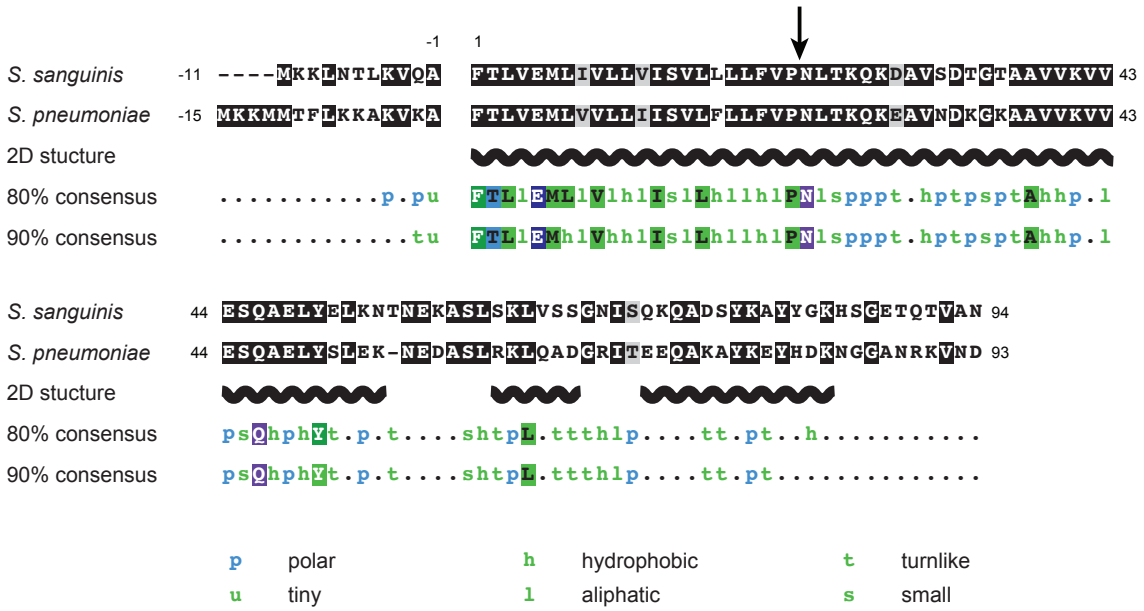

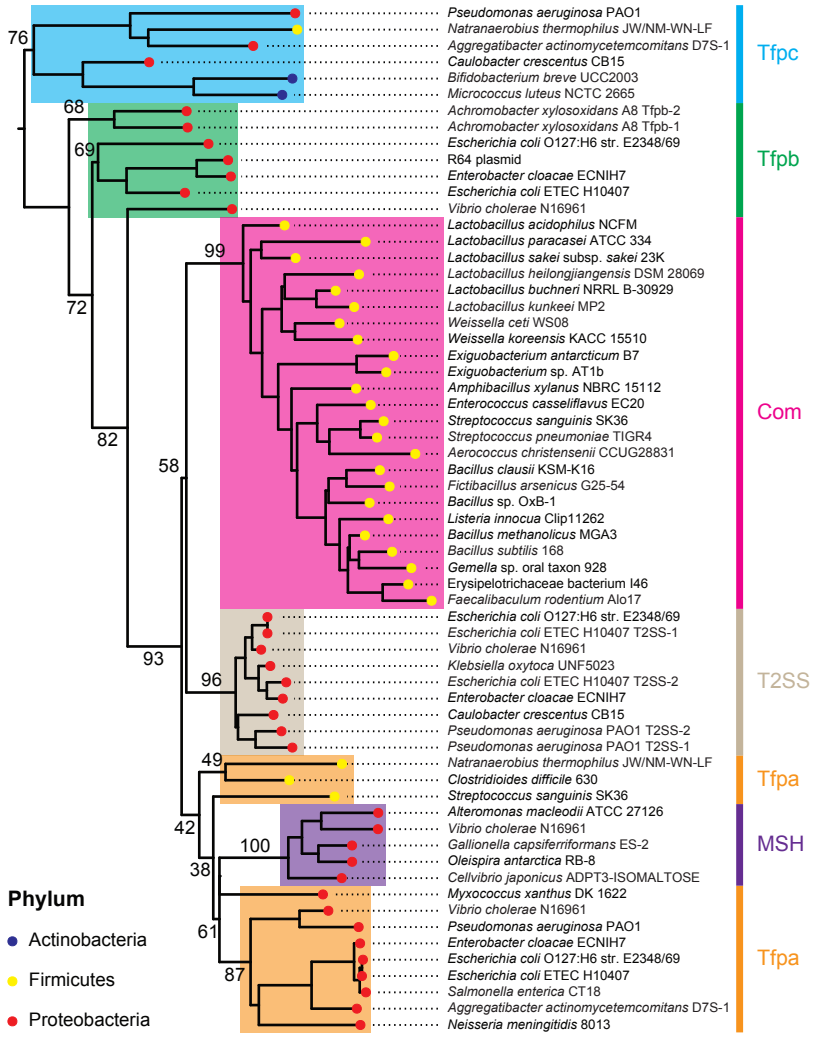

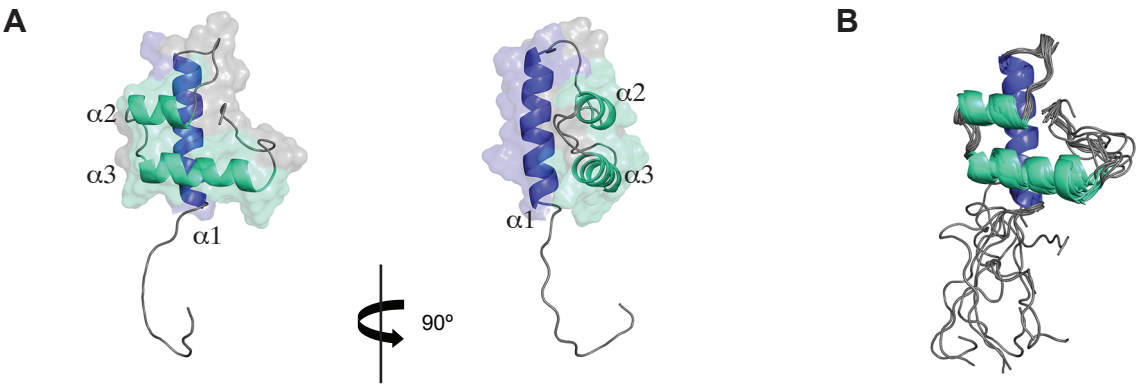

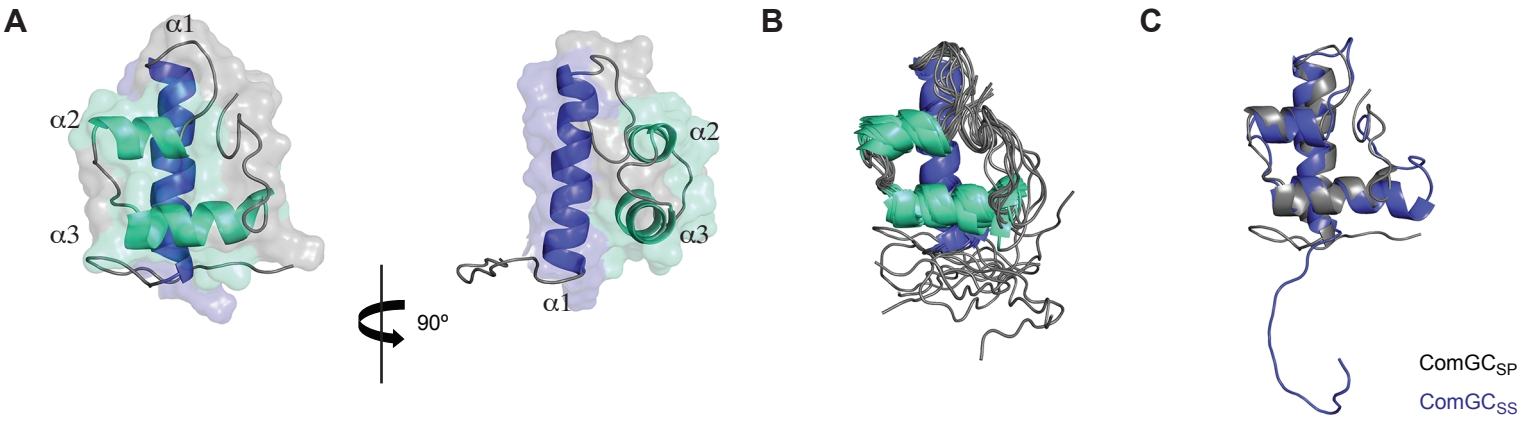

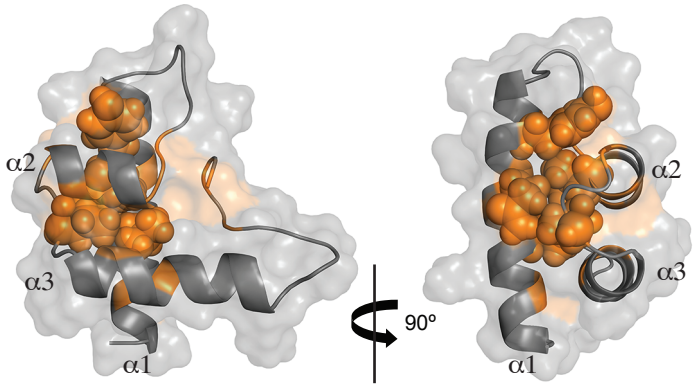

N. gonorrhoeae PilE

G. sulfurreducens PilE

S. sanguinis ComGC